Glycobiology, 2020, vol. 30, no. 10, 802–816
doi: 10.1093/glycob/cwaa029
Advance Access Publication Date: 5 April 2020
Original Article

Cancer Biology

Catfish egg lectin affects influx and efflux rates of sunitinib in human cervical carcinoma HeLa cells

Shigeki Sugawara[2], Madoka Takayanagi[2,3], Shota Honda[2], Takeo Tatsuta[2], Yuki Fujii[4], Yasuhiro Ozeki[5], Jun Ito[6], Makoto Sato[6], and Masahiro Hosono[2,1]

[2]Division of Cell Recognition Study, Institute of Molecular Biomembrane and Glycobiology, Tohoku Medical and Pharmaceutical University, 4-4-1 Komatsushima, Aoba-ku, Sendai 981-8558, Japan, [3]Chemiluminescent Reagents Department, R&D Section, Kagamida Factory, DENKA SEIKEN Co. Ltd., 1359-1 Kagamida, Kigoshi Gosen-shi, Niigata 959-1695, Japan, [4]Graduate School of Pharmaceutical Sciences, Nagasaki International University, 2825-7 Huis Ten Bosch, Sasebo, Nagasaki 859-3298, Japan, [5]Department of Life and Environmental System Science, Laboratory of Glycobiology and Marine Biochemistry, Graduate School of NanoBio Sciences, Yokohama City University, 22-2 Seto, Kanazawa-ku, Yokohama 236-0027, Japan, and [6]Department of Urology, Faculty of Medicine, Tohoku Medical and Pharmaceutical University, 1-15-1 Fukumuro, Miyagino-ku, Sendai 983-8536, Japan

[1]To whom correspondence should be addressed: Tel: +81-22-727-0114; Fax: +81-22-727-0092; e-mail: mhosono@tohoku-mpu.ac.jp

Received 15 August 2019; Revised 24 March 2020; Editorial Decision 24 March 2020; Accepted 24 March 2020

Abstract

New treatment protocols are aiming to reduce the dose of the multitargeted tyrosine kinase inhibitor sunitinib, as sunitinib elicits many adverse effects depending on its dosage. *Silurus asotus* egg lectin (SAL) has been reported to enhance the incorporation of propidium iodide as well as doxorubicin into Burkitt's lymphoma Raji cells through binding to globotriaosylceramide (Gb3) on the cell surface. The objective of this study was to examine whether SAL enhances the cytotoxic effect of sunitinib in Gb3-expressing HeLa cells. Although the treatment with SAL delayed the cell growth and enhanced the propidium iodide uptake, cell death accompanied by membrane collapse was not observed. The viability of sunitinib-treated HeLa cells was significantly reduced when the treatment occurred in combination with SAL compared to their separate usage. Sunitinib uptake significantly increased for 30 min in SAL-treated cells, and this increment was almost completely abolished by the addition of L-rhamnose, a hapten sugar of SAL, but not by D-glucose. After removal of SU from the medium, the intracellular sunitinib level in SAL-treated cells was higher than in untreated cells for 24 h, which was not observed in Gb3-deficient HeLa cells. Furthermore, we observed that SAL promoted the formation of lysosome-like structures, which are LAMP1 positive but not acidic in HeLa cells, which can trap sunitinib. Interestingly, SAL-induced vacuolation in HeLa cells was not observed in another Gb3 positive Raji cells. Our findings suggest that SAL/Gb3 interaction promoted sunitinib uptake and suppressed sunitinib excretion and that sunitinib efficiently exerted cytotoxicity against HeLa cells.

Key words: globotriaosylceramide, rhamnose-binding lectin, sunitinib, vacuolation

Introduction

Conventional cancer chemotherapy is often associated with the risk of adverse drug reactions such as blood disorders due to bone marrow suppression, nausea/vomiting, diarrhea/constipation and pain, all of which reduce the quality of life of cancer patients (Carelle et al. 2002). The main disadvantage of this treatment is that most anticancer drugs do not always specifically target cancer cells. Hence, development of drugs targeting molecules specifically or predominantly expressed in cancer cells, but not in normal cells, is an active area of research. These approaches, based on molecular, cellular, biochemical and immunological methods, have succeeded in producing a variety of targeted molecule-specific anticancer drugs.

Tyrosine kinases (TKs), known to be involved in cell proliferation and differentiation, are overexpressed in certain types of cancer cells (Sawyers 2004). Therefore, TK is currently an effective therapeutic target for cancer chemotherapy, and many compounds that inhibit TKs have been developed so far. Sunitinib (SU, SUTENT®) is a TK inhibitor that targets vascular endothelial growth factor receptor (VEGFR)-1, VEGFR-2, VEGFR-3, platelet-derived growth factor receptor (PDGFR)α/PDGFRβ, tyrosine protein kinase kit (c-kit) and fms-related TK 3 (Abrams et al. 2003; Mendel et al. 2003; Croci et al. 2014). SU is mainly used for the treatment of metastatic renal cell carcinoma (mRCC); it also exerts a cytotoxic effect in a variety of solid tumors, for example, gastrointestinal stromal tumor and pancreatic neuroendocrine tumors (Demetri et al. 2006; Raymond et al. 2011; Boegemann et al. 2018). However, SU is also known to cause many adverse effects such as anemia, lymphopenia, neutropenia, thrombocytopenia and leucopenia, depending on its dosage (Aparicio-Gallego et al. 2011). Therefore, development of alternative treatment protocols that can reduce the dose of SU is urgently required.

Silurus asotus egg lectin (SAL), belonging to the rhamnose-binding lectin (RBL) family, is found in catfish eggs and is capable of binding to globotriaosylceramide (Gb3) in glycosphingolipid-enriched microdomains (GEM) on the cell membrane (Hosono et al. 1993; Hosono et al. 1999; Kawano et al. 2009; Hosono et al. 2013). We have previously shown that SAL decreased the survival rate of Gb3-expressing Burkitt's lymphoma Raji cells by inducing G0/G1 phase arrest (Sugawara et al. 2017). Furthermore, we showed that SAL promoted propidium iodide (PI) uptake into Raji cells (Sugawara, Hosono, et al. 2005). Although the apparent molecular mechanism of this effect has not been elucidated, we conducted further studies and demonstrated that SAL also increases the uptake of doxorubicin (Dox) into Raji cells and consequently enhances the cytotoxic effect of Dox (Sugawara, Sasaki, et al. 2005). The combined use of SAL halved the dose of Dox required to attain cell viability similar to that observed in its single treatment (Sugawara et al. 2011). In addition, we showed that the cytotoxic effects of vinblastine (VBL) and irinotecan (CPT-11) were significantly increased in SAL-pretreated Raji cells (Sugawara et al. 2011). These results suggest that the combined use of SAL and other chemotherapeutic drugs resulted in an additive or synergistic effect between anticancer agents in Gb3-expressing cancer cells, which may lead to the reduction in their therapeutic dose.

Tekisogullari and Topcul (2013) and Shin et al. (2009) reported that SU reduces the viability of human cervical cancer HeLa cells, which express Gb3 on their surface (Tekisogullari and Topcul 2013; Shin et al. 2009). In this study, we observed that SAL significantly decreased the viability of HeLa cells in combination with SU and revealed two underlying mechanisms involved in this phenomenon: an increase in uptake and a decrease in efflux. SAL enhanced SU incorporation via binding to the carbohydrate moiety of Gb3 and subsequently induced accumulation of SU in the vacuole membrane newly formed after SAL pretreatment of HeLa cells. Our observations provide some important insights into lectin-combinatorial cancer chemotherapy.

Results

Effects of SAL on HeLa cells

We have previously reported that SAL significantly increased PI incorporation in Raji cells and decreased their proliferation without inducing cell death (Sugawara, Hosono, et al. 2005; Sugawara et al. 2017). According to the results from flow cytometric analysis, PI incorporation also increased in SAL-treated HeLa cells (Figure 1A). PI cannot normally permeate membranes of live cells, and PI incorporation usually follows membrane collapse in cells at the late apoptotic or necrotic phase (Tsujimoto 1997). The WST-8 assay showed that the viability of SAL-treated HeLa cells was reduced to 82% (Figure 1B). However, this method does not directly reflect the proliferative ability. Therefore, we investigated whether SAL reduced cell proliferation using the RealTime-Glo^{MT} cell viability assay reagent, which is capable of monitoring the number of living cells in culture in real time. As shown in Figure 1C, SAL reduced cell proliferation in a time-dependent manner. Additionally, lactate dehydrogenase (LDH) leakage was not detected in cells treated with SAL for 24 h (Figure 1D), and the morphology of HeLa cells did not change at a concentration of SAL up to 200 μg/mL (Supplementary Figure S1). Hence, these results suggest that SAL induces PI uptake in HeLa cells without membrane collapse-associated cell death as observed in Raji cells.

Combined effect of SAL and SU in HeLa cells

Based on previous studies, we predicted that SAL may increase the incorporation of certain small molecule drug, such as Dox, in HeLa cells (Supplementary Figure S2).

Hence, we tested the cytotoxic effect of SU on HeLa cells. SU treatment reduced the viability of HeLa cells in a dose-dependent manner (Figure 2A, left panel). As 12.5 and 25 μM SU moderately decreased cell viability to 80 and 50%, respectively, we used these concentrations for the subsequent combination assay. As shown in Figure 2A (right panel), pretreatment with SAL (50 μg/mL) enhanced the toxicity of SU by reducing cell viability to 51 and 26%, respectively. Furthermore, the cytotoxicity-promoting effects of SAL were reversed by the addition of L-rhamnose, the most potent inhibitory sugar, but not by D-glucose (Figure 2B). Therefore, SAL may act in combination with SU against HeLa cells via a carbohydrate-binding manner.

Alteration of SU influx and efflux by SAL

To elucidate the mechanism by which the effect of SU is enhanced in SAL-treated HeLa cells, we analyzed the content of intracellular SU utilizing its autofluorescence (Nowak-Sliwinska et al. 2015). As shown in Figure 3A, SU was incorporated in proportion to its concentration. The intracellular SU content increased after SAL treatment, which was abolished in the presence of L-rhamnose but not D-glucose (Figure 3B). To further determine whether SAL affects SU efflux, we temporally observed the residual amount of intracellular SU after

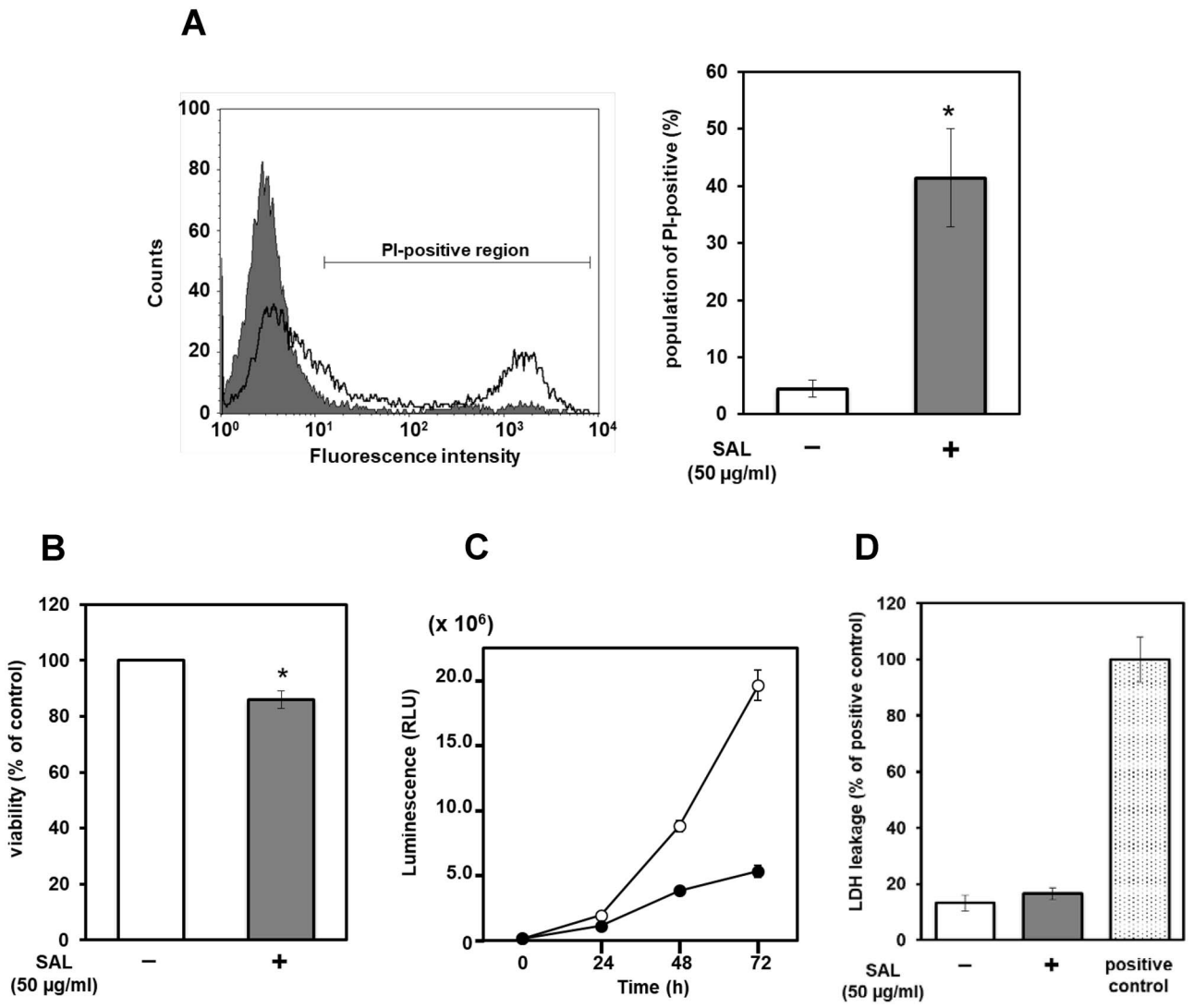

Fig. 1. SAL accelerates PI incorporation and reduces proliferation, but has no cytotoxic effect on HeLa cells. (**A**) Cells (1×10^5) were treated with (solid line) or without (shaded histogram) SAL (50 μg/mL) for 24 h at 37°C. Population of PI-positive cells was determined using FACSCalibur (left panel). The right panel shows the percentage of PI-positive cells. (**B**) Cells (5×10^3) were treated with (+) or without (−) SAL (50 μg/mL) for 48 h at 37°C. Cell viability was assessed using the WST-8 assay. (**C**) Cells (5×10^2) were treated with (closed circles) or without (open circles) SAL (50 μg/mL) at 37°C for 0, 24, 48 and 72 h. Cell growth was measured using the RealTime-Glo^{MT} viability assay. Luminescence was monitored after every 24 h for 3 d. (**D**) Cells (1×10^4) were cultured in a serum-free medium for 24 h. Subsequently, cells were treated with (+) or without (−) SAL (50 μg/mL) for 24 h at 37°C. Total intracellular LDH (positive control) was determined by incubating HeLa cells in lysis solution. LDH leakage was measured using CytoTox-ONE homogeneous membrane integrity assay. Each value represents the mean value ± SE for three independent experiments performed in triplicate. $^*P < 0.05$ vs. untreated control cells. This figure is available in black and white in print and in colour at Glycobiology online.

removing it from the culture medium using confocal laser scanning microscopy. Only weak SU fluorescence was detected in control HeLa cells 3 h after SU removal (Figure 3C). Conversely, intense fluorescence of residual SU was observed in SAL-treated cells even after 24 h. In the time-course analysis using the "Operetta" high-content imaging system (PerkinElmer, Hamburg, Germany), SU uptake reached a plateau level within 10 min in SAL-untreated cells but increased till 30 min to a significantly higher level in SAL-treated cells (Figure 3D). After removal of SU from the medium, the intracellular SU level in SAL-treated cells was higher than in untreated cells till 24 h. These results suggest that SAL promoted the influx but retarded the efflux of SU from HeLa cells. As SU is known to be excreted by the membrane transporter P-glycoprotein (P-gp) or breast cancer resistance protein (BCRP) (Kunimatsu et al. 2013), we assessed whether SAL altered the expression of P-gp and BCRP in HeLa cells. The expression of both transporters increased slightly but never decreased after SAL treatment (Figure 3E). In addition, SAL enhanced an influx of rhodamine (Rho) 123, a substrate of P-gp, but did not affect the efflux from HeLa cells (Supplementary Figure S3). Therefore, it is clear that the accumulation of SU is not because of the decrease in the expression nor in the activity of multidrug resistance transporters.

Incorporation of SU by Gb3/SAL interaction at the cell surface

Next, we knocked out α1,4-galactosyltransferase (A4GALT), also called Gb3 synthase, in HeLa cells to obtain a Gb3-deficient cell line (Gb3-KO). As shown in Figure 4A and B, Gb3 was hardly detected

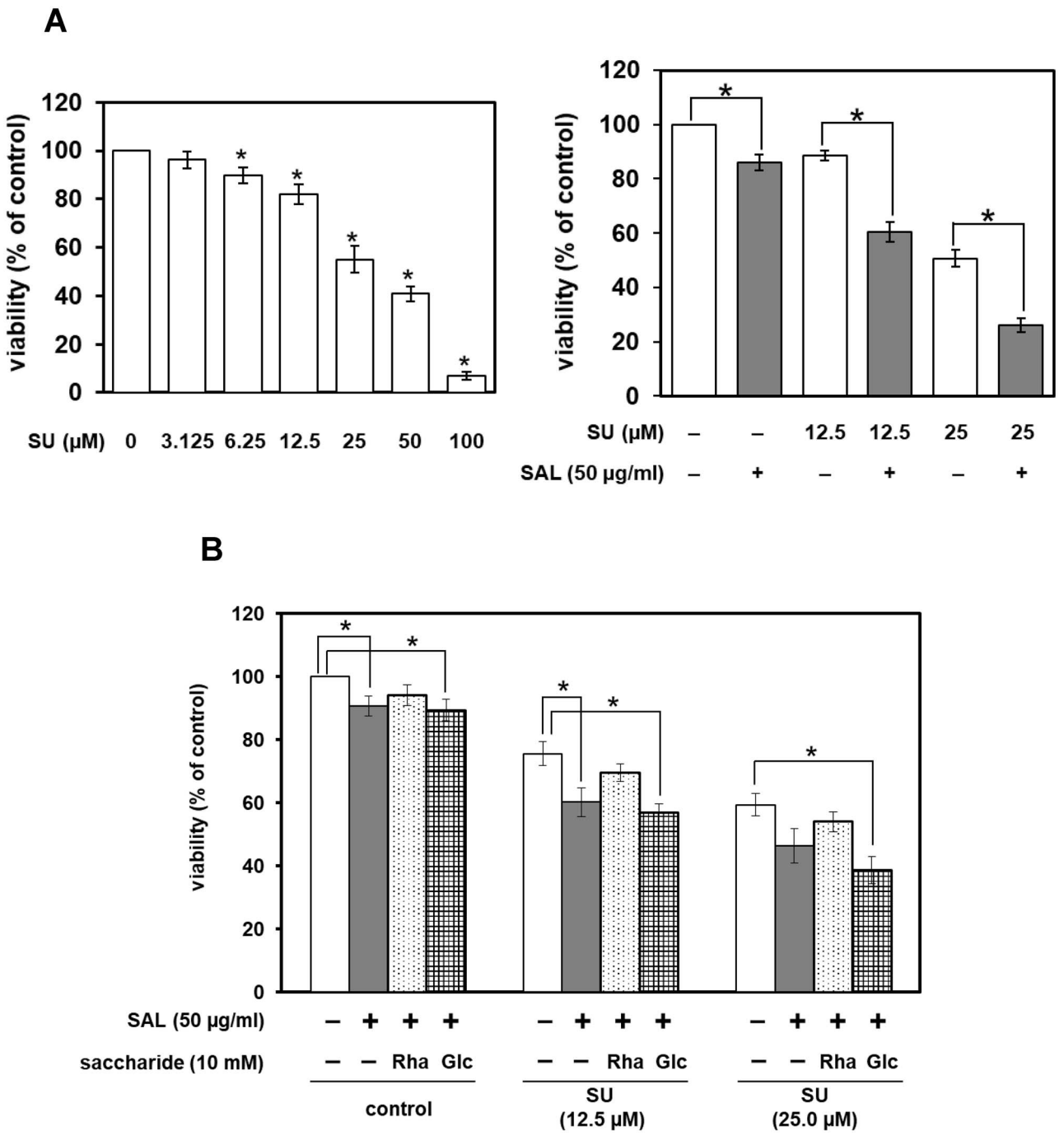

Fig. 2. SAL enhances the antitumor effects of SU on Hela cells. (**A**) Cells (5×10^3) were treated with SU (0, 3.12, 6.25, 12.5, 25, 50 and 100 μM) for 24 h at 37°C (left panel). Cells (5×10^3) were pretreated with SAL (0 and 50 μg/mL) for 24 h at 37°C. Then, SAL-pretreated cells were treated with SU (0, 12.5 and 25 μM) for 24 h at 37°C (right panel). (**B**) Cells (5×10^3) were pretreated with SAL (0 and 50 μg/mL) and SAL/saccharide (10 mM) for 24 h at 37°C. Then, SAL- and SAL/saccharide-pretreated cells were treated with SU (12.5 or 25 μM) for 24 h at 37°C. Cell viability was measured using the WST-8 assay. Each value represents the mean value ± SE for three independent experiments performed in triplicate. $^*P < 0.05$ vs. untreated control cells. This figure is available in black and white in print and in colour at Glycobiology online.

in the Gb3-KO cells compared to wild-type cells, and no change was observed in the proportion of PI-positive cells when both cells were treated with SAL (50 μg/mL, 24 h) (Figure 5A). The viability of Gb3-KO cells treated with SAL was also comparable to that of wild-type cells (Supplementary Figure S4). Although SU treatment decreased the viability of Gb3-KO cells in a dose-dependent manner (Figure 5B, left panel), similar to that in wild-type HeLa cells, the combined effect with SAL was abolished (Figure 5B, right panel). Furthermore, SU influx and efflux conditions after treatment with SAL were not altered in Gb3-KO HeLa cells (Figure 5C and D), indicating that the direct interaction between Gb3 and SAL promoted SU uptake and suppressed its excretion.

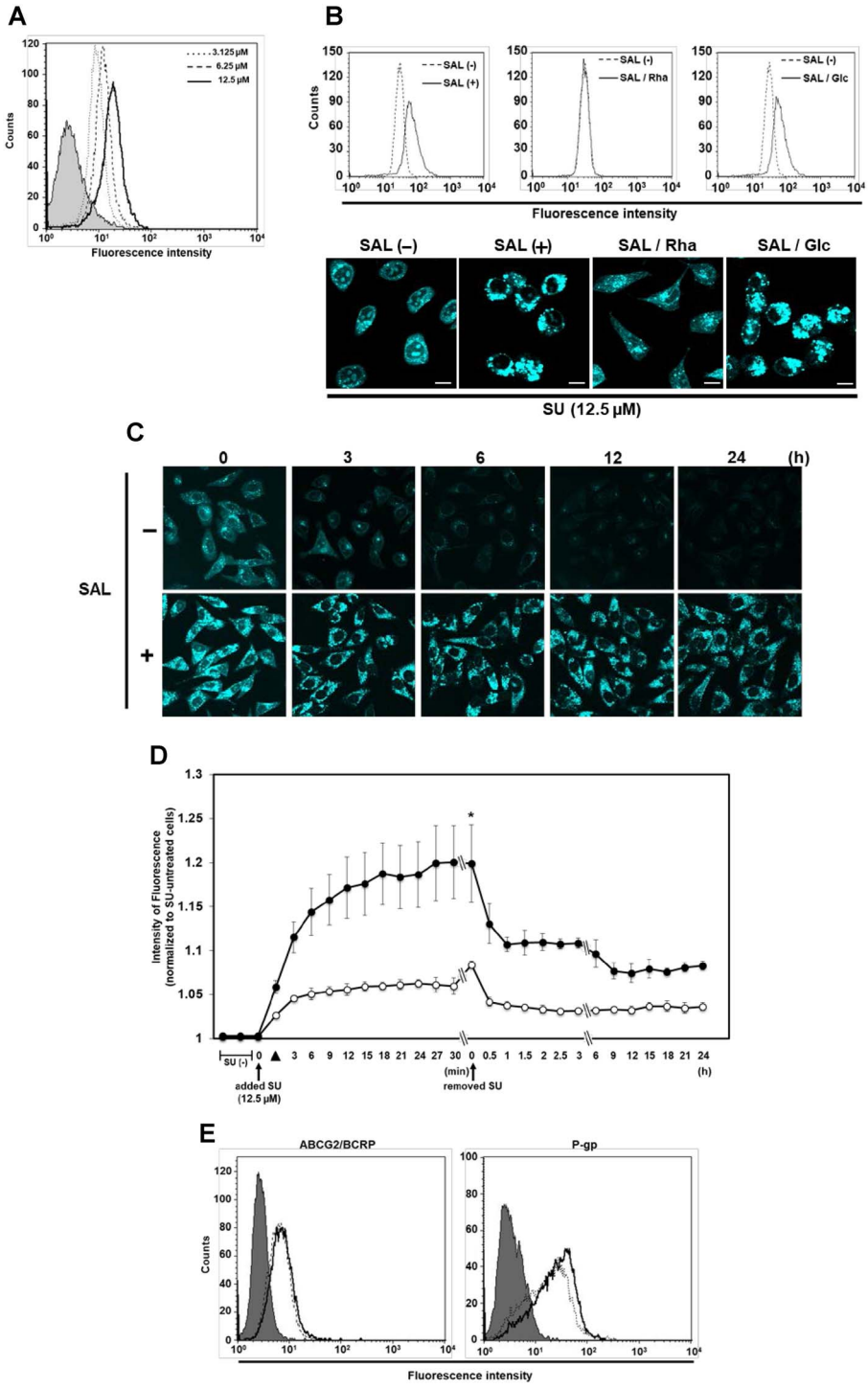

Fig. 3. SAL promotes SU influx and suppresses SU efflux in Hela cells. (**A**) Cells (1×10^5) were treated with SU (dotted line, 3.12 μM; broken line, 6.25 μM; solid line, 12.5 μM) for 30 min at 37°C. The autofluorescence of SU was detected using FACSCalibur. Fluorescence intensity of control cells: shaded histogram. (**B**) Cells (3×10^4) were pretreated with SAL (0 and 50 μg/mL) and SAL/saccharide (10 mM) for 24 h at 37°C. Subsequently, cells were treated with SU (12.5 μM) for 30 min at 37°C. Intracellular SU was detected using FACSCalibur (upper panels) and confocal laser scanning microscopy (lower panels). (**C**) Cells (3×10^4) were pretreated with or without SAL (50 μg/mL) at 37°C for 24 h. Thereafter, cells were treated with SU (12.5 μM) at 37°C for 30 min. After SU was removed from the medium, the residual quantity of SU in the cells was observed using confocal laser scanning microscopy at the indicated time points. SU is represented by a pseudo cyan color. (**D**) Time-course analysis was performed, in which the autofluorescence of SU in the cells was measured using Operetta CLS. HeLa cells were treated with (closed circles) or without (open circles) SAL (50 μg/mL) for 24 h at 37°C. Subsequently, these cells were treated with SU (12.5 μM). SU influx and efflux were analyzed every 3 min after SU was added to the medium at 0 min and after every 0.5 or 3 h after SU was removed from the medium at 0 h, respectively. The closed triangle indicates the time immediately after SU addition. (**E**) Cells (1×10^5) were pretreated with (solid line) or without (broken line) SAL (50 μg/mL) at 37°C for 24 h. BCRP and P-gp expression of SAL-treated HeLa cells were analyzed using anti-ABCG2 mAb and AF488-tagged goat anti-mouse mAb (left panel) and biotin-labeled P-gp-reactive MRK16 mAb and fluorescein isothiocyanate (FITC)-conjugated streptavidin (right panel), respectively. The degree of ABCG2/BCRP and P-gp expression on HeLa cell membranes was determined in the same way as described in (**A**). Fluorescence intensity of control cells: shaded histogram. Each value represents the mean value ± SE for three independent experiments performed in triplicate. $*P < 0.05$ vs. untreated control cells. Photographs were captured using a 60× objective lens. Scale bar, 10 μm. This figure is available in black and white in print and in colour at Glycobiology online.

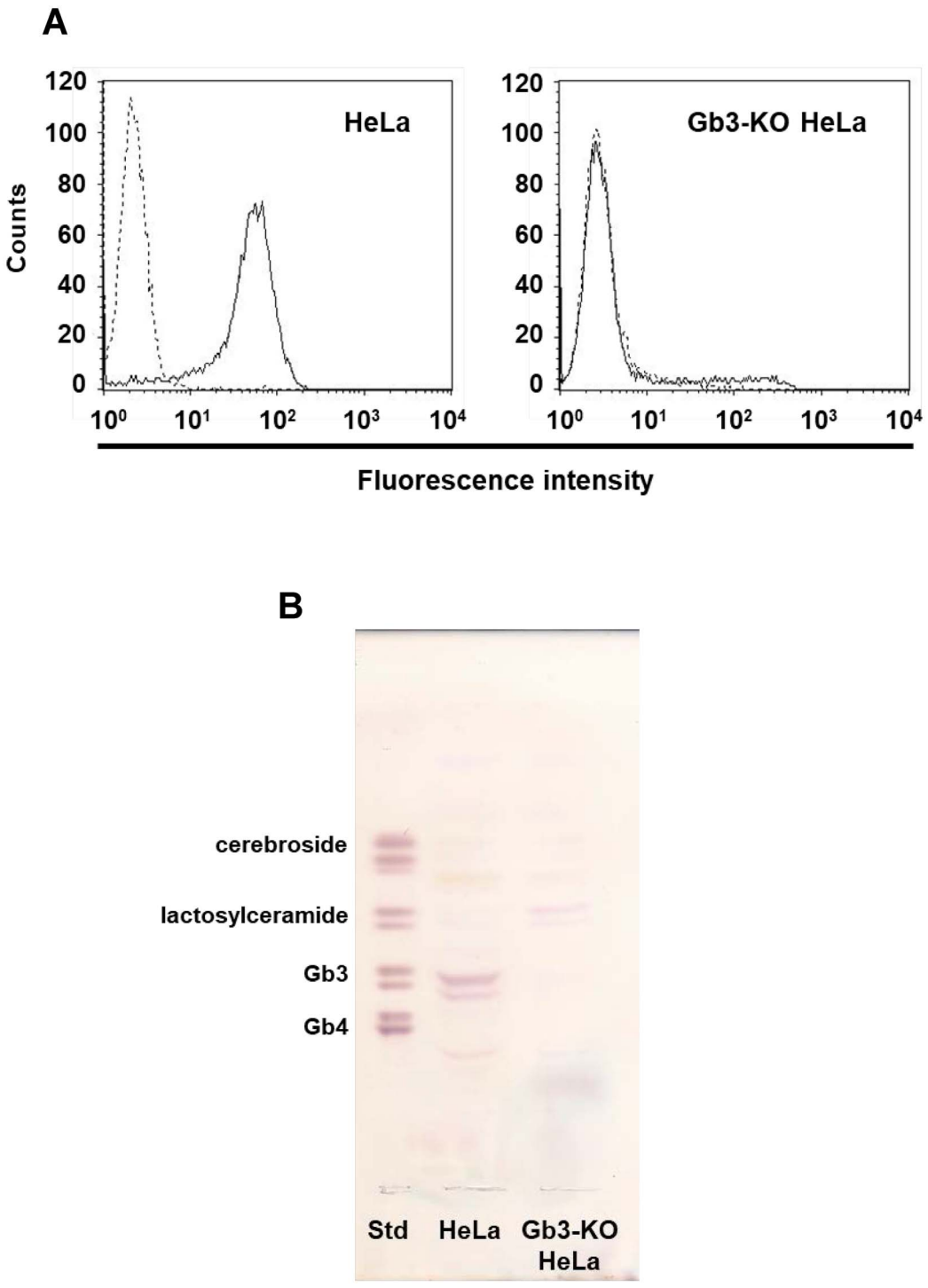

Fig. 4. Confirmation of Gb3 expression in HeLa and Gb3-KO HeLa cells. (**A**) Flow cytometric analysis of Gb3 on HeLa and Gb3-KO HeLa cells. Cells (2×10^5) were treated with anti-Gb3 mAb and AF488-tagged goat anti-mouse mAb (solid line). The degree of Gb3 expression on HeLa and Gb3-KO HeLa cell membranes was determined using FACSCalibur. Fluorescence intensity of control cells: dashed line. (**B**) Total glycosphingolipids isolated from HeLa and Gb3-KO HeLa were separated on TLC using the solvent system described in Materials and methods, and TLC plates were visualized with orcinol-H_2SO_4 reagent. On the standard lane (Std), an aliquot of the standard mixture containing cerebrosides, lactosylceramide, Gb3 and Gb4 was developed. This figure is available in black and white in print and in colour at Glycobiology online.

Alteration of intracellular distribution of SU by SAL in HeLa cells

Figure 3 shows that SAL influenced the uptake and excretion of SU. To gain insight regarding the mechanism of SAL-induced suppression of SU efflux from HeLa cells, we focused on the distribution of SU with and without treatment with SAL. The fluorescence of SU was widely distributed as "dots" in the cytosol of SAL-untreated HeLa cells, whereas a number of characteristic "circular"

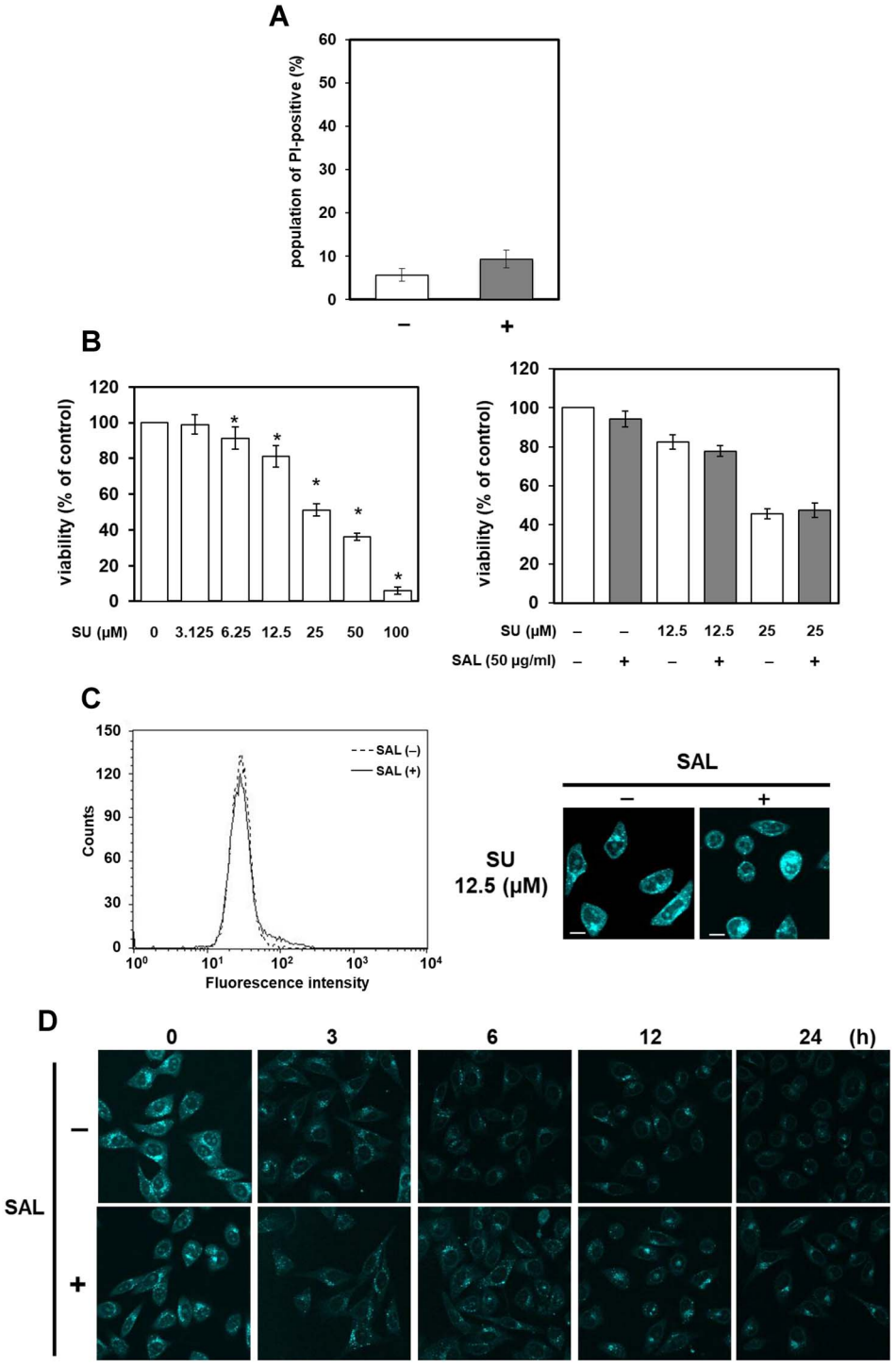

Fig. 5. SAL does not enhance the antitumor effects of SU on G3-KO HeLa cells. (**A**) Gb3-KO HeLa cells (1×10^5) were treated with (+) or without (−) SAL (50 μg/mL) for 24 h at 37°C. Population of PI-positive cells was determined using FACSCalibur. (**B**) Gb3-KO HeLa cells (5×10^3) were treated with SU (0, 3.12, 6.25, 12.5, 25, 50 and 100 μM) for 24 h at 37°C (left panel). Gb3-KO HeLa cells (5×10^3) were pretreated with SAL (0 and 50 μg/mL) for 24 h at 37°C. Then, SAL-pretreated cells were treated with SU (0, 12.5 and 25 μM) for 24 h at 37°C (right panel). Cell viability was determined using the WST-8 assay. (**C**) Gb3-KO HeLa cells (3×10^4) were pretreated with (+) or without (−) SAL (50 μg/mL) for 24 h at 37°C. Subsequently, the cells were treated with SU (12.5 μM) for 30 min at 37°C. Intracellular SU was detected using FACSCalibur (left panel) and confocal laser scanning microscopy (right panels). (**D**) Cells (3×10^4) were pretreated with (+) or without (−) SAL (50 μg/m) at 37°C for 24 h. Thereafter, the cells were treated with SU (12.5 μM) at 37°C for 30 min. After SU was removed from the medium, the residual quantity of SU in the cells was detected using confocal laser scanning microscopy. SU is represented by a pseudo cyan color. Each value represents the mean value ± SE for three independent experiments performed in triplicate. $^*P < 0.05$ vs. untreated control cells. Photographs were captured using a 60× objective lens. Scale bar, 10 μm. This figure is available in black and white in print and in colour at Glycobiology online.

structures consisting of SU fluorescence were observed in SAL-treated cells (Figure 6A). Interestingly, these remarkable vacuole-like structures appeared to "trap" SU and accumulated in HeLa cells; however, they were not observed in SAL-treated Raji cells (Supplementary Figure S5). Although it is still unclear what caused this difference in these cell lines, one possibility might be due to the difference in SAL-induced changes of signal transduction involved in MEK-ERK pathway as described in discussion section, or in the intracellular trafficking mechanisms of SAL. Next, we investigated the mechanism of SAL-induced vacuolation. The vacuoles were formed 9 h after SAL treatment (Figure 6B) and disappeared when SAL was removed from the cell surface by L-rhamnose treatment (Figure 6C). It is known that intracellular SU is sequestered in acidic lysosome compartments of cancer cells (Gotink et al. 2011). We stained various organelles to identify the vacuoles specifically induced by SAL in HeLa cells. As a result, the vacuoles were not stained with Nile Red nor with LysoTracker Green, marker dyes for lipid droplets and acidic organelles such as lysosome, respectively (Supplementary Figures S6 and S7). In addition, the expression of LC3, a marker of the autophagosome, was not observed in the SAL-induced vacuole membrane (Supplementary Figure S8). On the other hand, the vacuoles were stained reddish-brown by Neutral Red, a pH indicator that changes color from red to yellow between pH 6.8 and 8.0, indicating that the pH inside the vacuoles was near neutral (Figure 7A). Lysosomal-associated membrane protein 1 (LAMP1) is a lysosome marker. Although the vacuole might not be a lysosome per its internal pH, we assessed the existence of LAMP1 in the vacuole membrane by constructing HeLa cells transiently expressing a green fluorescence protein (GFP)-tagged LAMP1. As shown in Figure 7B, images similar to that shown in Figure 6A were obtained with the GFP-labeled LAMP1. In SAL-untreated HeLa cells, LAMP1 (lysosomes) was distributed in the cytosol in a "dotted" pattern, whereas characteristic "greenish circles" were observed in SAL-treated cells, indicating that SAL-induced vacuoles could simultaneously contain LAMP1 and SU. To confirm this, the red fluorescence protein (RFP)-labeled LAMP1 was used for double staining with SU. In SAL-treated HeLa cells, SU (cyan) and LAMP1 (magenta) colocalized around the vacuoles (white) (Figure 7C). Lysosomes are known to be derived from the Golgi apparatus (Saftig and Klumperman 2009), and brefeldin A (BFA), an intracellular protein transport inhibitor, was reported to prevent the budding of vesicles from the Golgi complex (Fujiwara et al. 1988; Reaves and Banting 1992). As shown in Figure 7D, BFA inhibited the formation of vacuoles in SAL-treated cells. Furthermore, it was found that the internalized SAL was localized around the vacuoles in the vicinity of nucleus (Figure 7E). From these results, we concluded that the vacuoles formed by SAL in HeLa cells could be lysosome-like organelles derived from the Golgi complex, which contain LAMP1, although their internal environment is not acidic. In addition, the internalized SU molecules are possibly trapped in the SAL-induced vacuole membrane, which is one of the reasons why SAL acts synergistically with SU.

Discussion

In this study, we showed that SAL retards the proliferation of HeLa cells without inducing cell death, but enhances the cytotoxic effect of SU. We proposed a novel function of this lectin involving intracellular vacuolation, which increases SU influx and its retention in the cytosol, where it is sequestered in the vacuole membrane of human cervical carcinoma HeLa cells. This indicates that SAL may be used for combined cancer chemotherapy.

Combination chemotherapy is known to be more effective than monotherapy for treating cancer patients. Usually, two or more drugs elicit different effects due to differences in their target receptors, mechanisms of action and effects on the cell cycle. The benefits of combination therapy include reduction in adverse effects, acquired drug resistance and the dose of each drug used in the treatment. However, it is associated with the potential hazard of drug interactions and certain unexpected side effects. Therefore, lowering the dosage of anticancer drugs via combined therapy is one of the targets of cancer chemotherapy.

In our previous study, we showed that SAL suppresses the proliferation of Gb3-expressing Raji cells and that the molecular mechanism involves an increase in the expression of p21 due to the activation of the mitogen-activated protein/extracellular signal-regulated kinase (ERK) kinase (MEK)-ERK (MEK-ERK) pathway (Sugawara et al. 2017). However, this pathway was not activated in HeLa cells (Supplementary Figure S9). Hence, proliferation of SAL-treated HeLa cells may be suppressed via a mechanism that is different from that of Raji cells. We first suspected that cell membrane collapse may be responsible for the promotion of SU uptake in HeLa cells because PI uptake was increased in SAL-treated cells, which is usually observed in the necrotic or late apoptotic phase of cell death (Figure 1A). However, significant reduction in cell viability and leakage of LDH were not observed in HeLa cells (Figure 1B and D), and hence we concluded that SAL promotes SU uptake without causing cell death or membrane collapse, which is an intriguing observation. CEL-III, a galactose-binding lectin derived from the marine invertebrate *Cucumaria chinate*, binds to sugar chains on the cell surface and causes hemolysis by forming an oligomeric transmembrane pore for the passage of low molecular compounds (Hatakeyama et al. 1995; Hatakeyama et al. 1996; Yamashita et al. 2011; Unno et al. 2014). As SAL is composed of three tandemly repeated carbohydrate recognition domains and forms a trimer in aqueous solution (Murayama et al. 1997), it might possibly form a pore in the cell membrane to promote SU uptake. Furthermore, studies show that the white salmon egg lectin (CSL3) of the RBL family increases the permeability of the fluorescent dye Lucifer Yellow by opening the tight junction of Caco-2 cells (Nemoto et al. 2015). Thus, interaction of lectin with the cell membrane via binding to carbohydrate chains may possibly modify the membrane function. The detailed mechanism of SAL-induced transport will be addressed in the next investigation.

Many cancer cells express adenosine triphosphate (ATP)-binding cassette (ABC) transporters that excrete drugs outside the cells (Domenichini et al. 2019). SAL enhances the cytotoxic effect of antitumor drugs in Raji cells by decreasing the expression of multidrug resistance-associated protein 1 (MRP1), an ABC transporter (Fujii, Sugawara, et al. 2012a). Reports show that P-gp and BCRP are responsible for the efflux of SU in certain tissues (Gotink et al. 2011). In HeLa cells, P-gp and BCRP were expressed in the plasma membrane (Figure 3E), via which the incorporated SU molecules (12.5 μM for 30 min treatment) might be excreted outside within 3 h. However, P-gp and BCRP expression on the membrane increased only slightly after SAL treatment (Figure 3E). In addition, MDR1-P-gp kept its activity after treatment of SAL (Supplementary Figure S3) as described above. Based on these results, we concluded that SU accumulation effect of SAL was at least exerted beyond the capacities of these transporters. Based on these results, we concluded that these transporters may not be involved in regulating the intracellular SU concentration even after 24 h (Figure 3C).

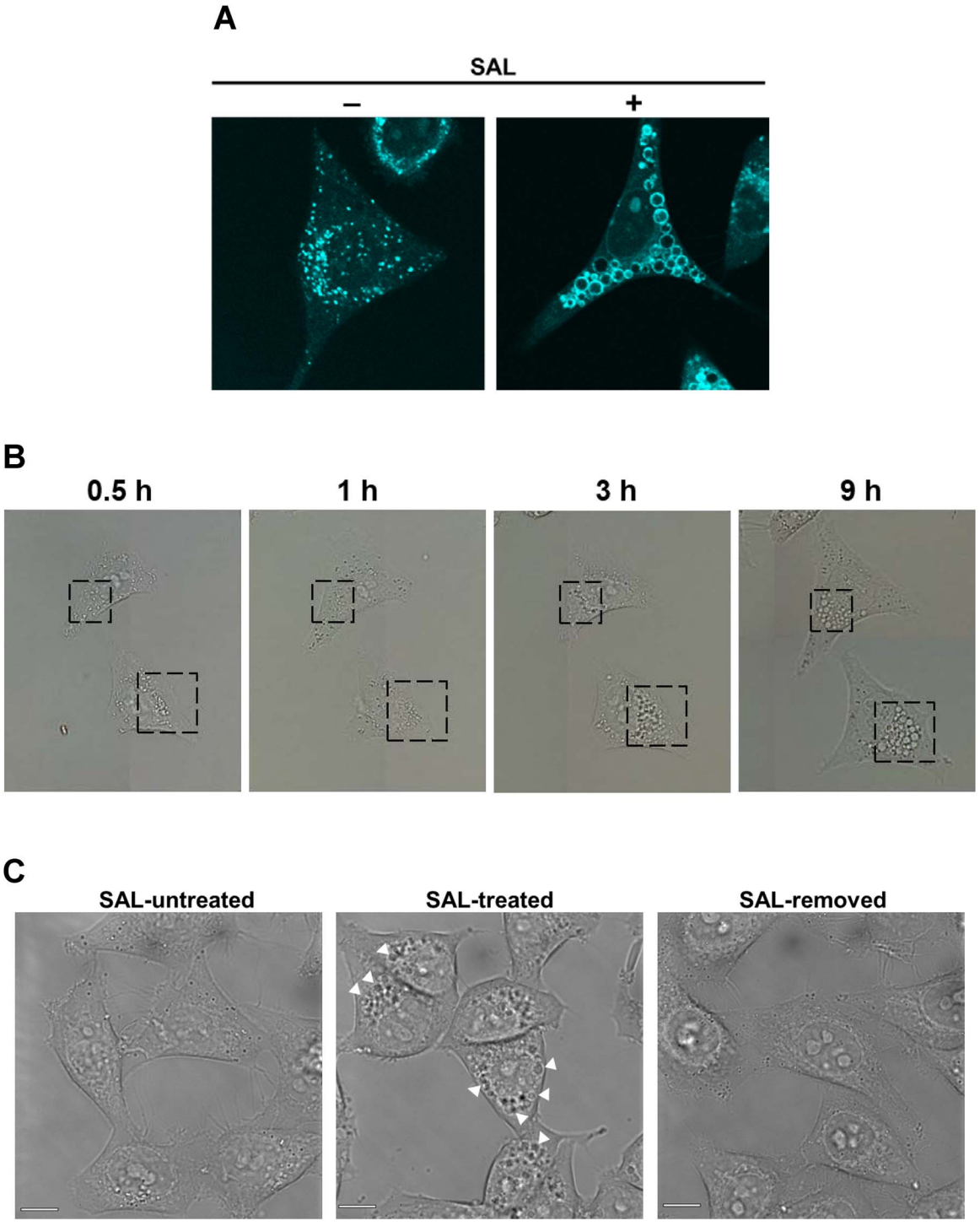

Fig. 6. SAL alters the accumulation profile of SU in HeLa cells. (**A**) Cells (3×10^4) were pretreated with (+) or without (−) SAL (50 μg/mL) for 24 h at 37°C. Thereafter, the cells were treated with SU (12.5 μM) for 30 min at 37°C. The fluorescence of SU was detected using confocal laser scanning microscopy. Photographs were captured using a 60× objective lens with 4× scan zoom. (**B**) Vacuole production was observed between 0.5 and 9 h after treatment with SAL (50 μg/mL). The images are from bright-field microscopy at 60× magnification. (**C**) Cells (5×10^3) were cultured with (SAL-treated) or without (SAL-untreated) SAL (50 μg/mL) for 48 h. Other cells were treated with SAL (50 μg/mL) for 24 h, following which, the SAL bound to the cell membrane was removed with L-rhamnose, and the cells were again cultured in SAL-free medium for 24 h (SAL-removed). Formation of large vacuoles (solid white arrowheads) was detected using an inverted microscope. Photographs were captured using a 100× objective lens. Scale bar, 10 μm. This figure is available in black and white in print and in colour at Glycobiology online.

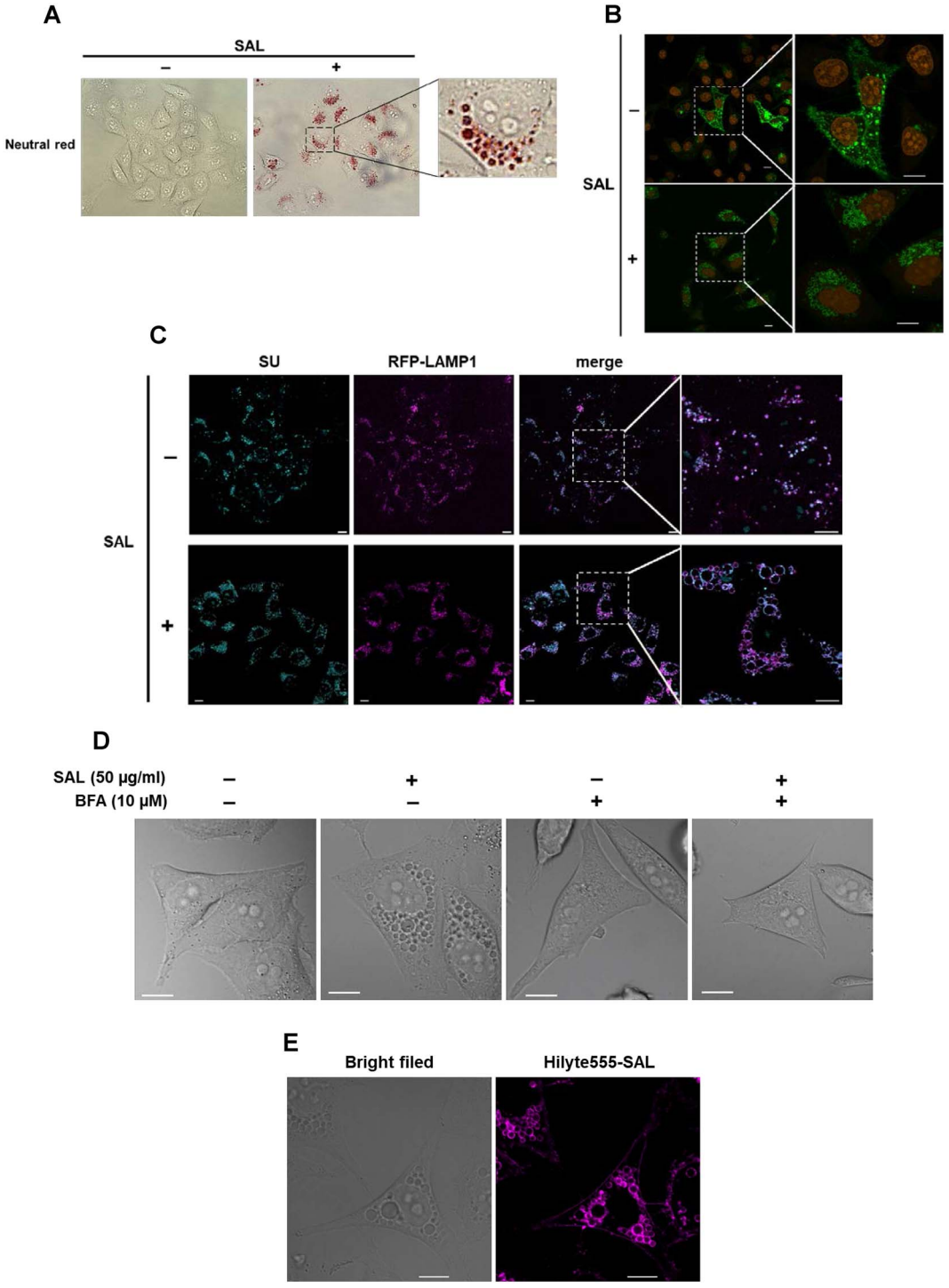

Fig. 7. SAL induces the formation of lysosome-like organelles in HeLa cells. (**A**) Cells (3×10^4) were treated with (+) or without (−) SAL (50 μg/mL) for 24 h at 37°C. Then, cells were exposed to Neutral Red for 30 min. Neutral Red was detected at the same time using the EVOS FL Auto 2 cell imaging system. (**B**) HeLa-LAMP1-GFP cells were pretreated with (+) or without (−) SAL (50 μg/mL) for 24 h at 37°C. Fluorescence of LAMP1-GFP (pseudo green color) was detected using confocal laser scanning microscopy. Nuclei were counterstained with DRAQ5 (pseudo orange color) Scale bar, 10 μm. (**C**) HeLa-LAMP1-RFP cells were pretreated with (+) or without (−) SAL (50 μg/mL) for 24 h at 37°C. Thereafter, the cells were treated with SU (12.5 μM) at 37°C for 30 min. Fluorescence of LAMP1-RFP (pseudo magenta color) and SU (pseudo cyan color) was detected using confocal laser scanning microscopy. Scale bar, 10 μm. (**D**) Cells (1×10^4) were treated with BFA (10 μM) in RPMI-1640 with FBS for 2 h, followed by addition of SAL (50 μg/mL) for 24 h. The images are from bright-field microscopy captured using a 60× objective lens. Scale bar, 10 μm. (**E**) Cells (3×10^4) were treated with HL-SAL (50 μg/mL) for 24 h at 37°C. Then, fluorescence of SAL (magenta) was observed using confocal laser scanning microscopy. Photographs were captured using a 60× objective lens with 3× scan zoom. Scale bar, 10 μm. This figure is available in black and white in print and in colour at Glycobiology online.

Owing to a significant difference in the intracellular distribution pattern of SU in the presence or absence of SAL, we presumed that SU efflux is prevented by the accumulation of SU in unidentified lysosome-like vacuoles formed by the binding of SAL to Gb3. MytiLec isolated from the mussel *Mytilus galloprovincialis* is not RBL but has an affinity for Gb3 as well as SAL (Fujii, Dohmae, et al. 2012). MytiLec significantly decreased the viability of HeLa cells more than 2 μg/mL, unlike in SAL, whereas neither obvious cell death nor vacuole formation was observed less than 2 μg/mL (Supplementary Figure S10). When HeLa cells were treated with 1 μg/mL of MytiLec, a safe concentration for the cells, SU accumulation was not observed. On the other hand, pretreatment of MytiLec clearly inhibited SAL-induced SU accumulation (Supplementary Figure S11). Sorting nexins (SNXs), which belong to a novel family of phox homology (PX) domain-bearing proteins responsible for intracellular transport, are widely conserved across species from yeast to mammals, and at present, 33 mammalian SNXs have been identified (Cullen 2008). SNXs are involved in various cellular functions such as endocytosis, endosome transport and signal transduction and play a fundamental and essential function in the maintenance of intracellular homeostasis. Qin et al. (2006) showed that the overexpression of SNX10 in HeLa cells led to the formation of giant vacuoles (Qin et al. 2006). On the contrary, Xu et al. (2013) reported that SNX11 inhibits SNX10-induced vacuolation (Xu et al. 2013). We reasoned that SAL might induce the formation of vacuoles by changing the expression levels of SNX10 and SNX11; however, expression of neither genes was changed in SAL-treated HeLa cells (Supplementary Figure S12). Therefore, these molecules are not involved in SAL-induced vacuolation.

Furthermore, Lin et al. (2016) have reported that giant vacuoles are formed after yttrium oxide nanoparticles are incorporated into HeLa cells via macropinocytosis (Lin et al. 2016). These vacuoles contain LAMP1 and their internal pH is almost neutral; thus, the properties of these vacuoles are similar to those formed by SAL treatment. It is still unclear if SAL is incorporated into HeLa cells. Further evidence is required to clarify the mechanism underlying SAL-induced vacuole formation.

Reports show that lysosomal sequestration of SU is one of the mechanisms by which tumor cells develop resistance. In fact, significantly more acidic lysosomes sequestering SU in the vacuoles are observed in resistant cells than in nonresistant cells (Gotink et al. 2011). However, SU was trapped "on" the vacuole membrane, i.e. in the cytosol, in the case of nonacidic SAL-induced cytoplasmic vacuoles. On the other hand, Tsai et al. (2017) reported that wheat germ agglutinin (WGA), with affinity for *N*-acetylglucosamine and sialic acid, induces cytoplasmic vacuolation and autophagic or paraptotic cell death in cervical cancer cell lines (Tsai et al. 2017). In addition, Pratt et al. showed that concanavalin-A (ConA) increases autophagic acidic vacuole formation through the intracellular membrane type-1 matrix metalloproteinase (MT1-MMP)-mediated signaling in glioblastoma cells (Pratt et al. 2012). Although such lectin-induced vacuolation may be relevant, it is clearly different from our observation, as SAL did not show any cytotoxicity via apoptotic and nonapoptotic cell death.

Recently, Di Desidero et al. (2017) reported that the combination of SU and CPT-11 showed significant and synergistic antitumor activity in undifferentiated thyroid cancer cells (Di Desidero et al. 2017). However, both drugs can affect normal cells and cause side effects. On the other hand, SAL has the advantage of selectively affecting Gb3-positive cells. It is known that Gb3 is one of the malignant markers overexpressing in the several tumor cells such as breast, ovarian, pancreatic, testicular and colorectal carcinoma (Ohyama et al. 1990; Kovbasnjuk et al. 2005; Wei et al. 2008; Maak et al. 2011; Stimmer et al. 2014). Although some limitations associated with the use of SAL need to be overcome, e.g. immunogenicity of SAL in vivo, as SAL itself is not cytotoxic but only suppresses proliferation, it might be a good candidate for combined cancer chemotherapy.

In conclusion, SAL suppresses cell proliferation, promotes the uptake of SU into cells and suppresses SU excretion in Gb3-positive Hela cells, because of which SU efficiently exerts cytotoxicity on HeLa cells. However, details of the mechanism underlying the formation of the unusual SAL-induced vacuoles remain unknown. Furthermore, the efficacy of SAL is mostly limited to Gb3-expressing cancer cells, which is possibly associated with malignant transformation (Lanne et al. 1996; Stimmer et al. 2014). In the future, SAL may be used for minimally invasive treatments after elucidating its mechanism of action and analyzing the combined effect of SAL and anticancer drugs on various cell types.

Materials and methods

Lectin and cell lines

SAL was purified according to the method described previously (Hosono et al. 1993). MytiLec was kindly gifted by Dr. Y. Ozeki, Yokohama City University, Yokohama, Japan. HeLa, a human cervical carcinoma cell line, obtained from the Cell Resource Center of Biomedical Research, Institute of Development, Aging and Cancer, Tohoku University (Sendai, Japan), was cultured in Roswell Park Memorial Institute (RPMI)-1640 medium (Nissui Pharmaceutical Co., Tokyo, Japan) supplemented with 10% v/v fetal bovine serum (FBS) and antibiotic–antimycotic solution (penicillin [100 IU/mL], streptomycin [100 μg/mL] and amphotericin B [0.25 μg/mL]; Life Technologies, Carlsbad, CA) and maintained at 37°C in a 95% air/5% CO_2 atmosphere.

Incorporation of PI in SAL-treated HeLa

Cells (2×10^5) were treated with or without 100 μL of SAL [50 μg/mL Dulbecco's phosphate-buffered saline (D-PBS)] or rat anti-Gb3 monoclonal antibody (mAb) (clone 38.13; Beckman Coulter, Miami, FL) at a dilution of 1:200 in D-PBS at 4°C for 30 min and washed thrice with D-PBS. Incorporation of PI was detected using the MEBCYTO apoptosis kit (MBL, Nagoya, Japan) and FACSCalibur (BD Biosciences, San Jose, CA).

Cell viability and proliferation assays

Cell viability was determined using the WST-8 assay and the cell counting kit-8 (CCK-8, Dojindo Laboratories, Kumamoto, Japan). After plating the cells into a 96-well flat-bottom plate at 5×10^3 cells/well (90 μL), the cells were treated with SAL (final concentration 50, 100 or 200 μg/mL) or MytiLec (final concentration 0.5, 1, 2, 10, 25 or 50 μg/mL) for 24 h. Next, the WST-8 solution (10 μL) was added into each well, and the cells were incubated for 4 h at 37°C. The absorbance was measured at a wavelength of 450 nm using the GloMax multidetection system (Promega, Madison, WI). Bright-field images were acquired using an inverted microscope (model IX71; Olympus, Osaka, Japan) with a 10 or 100× objective lens. Cell proliferation was determined using a RealTime-Glo^{MT} cell viability assay (Promega). Cells were grown in medium containing the RealTime-Glo^{MT} assay reagent and SAL (50 μg/mL). Proliferation

was monitored every 24 h for 3 d. The luminescence intensity was measured using the GloMax multidetection system (Promega).

Measurement of LDH

The LDH leakage assay was performed using the CytoTox-ONE homogeneous membrane integrity assay Reagent (Promega; Ivanova and Uhlig 2008). Cells (1×10^4) were seeded in a 96-well flat-bottom black plate (Nunc, Roskilde, Denmark) and cultured in serum-free medium for 24 h. Then, the cells were treated with SAL (final concentration 50 μg/mL) at 37°C for 24 h. Subsequently, 100 μL LDH assay reagent was added to each well, and the plates were incubated for 10 min at 22°C. The enzymatic reaction was stopped by adding 50 μL stop solution. LDH released in the extracellular environment was measured using a GloMax multidetection system (Promega) with an excitation wavelength of 525 nm and an emission wavelength of 590 nm. The maximum LDH release control (positive control) was set up by adding 2 μL lysis solution (9% Triton X-100) to control cells before the addition of reagent.

Flow cytometric analysis of Gb3 and ABC subfamily G member 2 (ABCG2)/BCRP expression

Cells (2×10^5) were treated with or without anti-Gb3 monoclonal antibody (mAb) (BGR23, mouse IgG2b; Tokyo Kasei Co. Ltd, Tokyo, Japan) at a dilution of 1:500 or anti-BCRP/ABCG2 mAb (5D3, mouse IgG2b; Santa Cruz Biotechnology, Dallas, TX) at a dilution of 1:200 in D-PBS (100 μL) at 4°C for 30 min and washed thrice with D-PBS. The cells were then treated with Alexa Fluor (AF) 488-conjugated goat anti-mouse IgG (H + L) (Molecular Probes, Invitrogen AG, Basel, Switzerland) at a dilution of 1:2500 in D-PBS (100 μL) at 4°C for 30 min. The degree of Gb3 or ABCG2/BCRP expression on the cell surface was analyzed using FACSCalibur (BD Biosciences).

Thin layer chromatography (TLC) for glycolipid expression analysis

Cells (1×10^6) were suspended in a solution of chloroform–methanol (2:1, v/v) and incubated for 1 h at 37°C, following which they were centrifuged at $1000 \times g$ for 10 min. The supernatant was recovered in a glass tube. The pellet was resuspended in a solution of chloroform–methanol–water (1:2:0.8, v/v) and treated for 2 h at 37°C, following which they were then centrifuged at $1000 \times g$ for 10 min. The supernatant was collected and evaporated to dryness under nitrogen gas. The residue was dissolved in 20 μL of chloroform–methanol (2:1, v/v), placed on a high-performance TLC (HPTLC) plate (Merck, Darmstadt, Germany) and developed using the solvent system of chloroform–methanol–water (60: 35: 8, v/v). Gb3 was visualized by spraying 0.5% orcinol in 10% sulfuric acid.

Analyzing the effect of the combination of SU and SAL

For determining the effect of SU, cells (5×10^3) were treated with SU (0, 3.12, 6.25, 12.5, 25, 50, and 100 μM) for 24 h at 37°C. For determining the effect of the SU and SAL combination, cells were incubated with SAL (50 μg/mL) in RPMI-1640 with FBS for 24 h, supplemented with SU (0, 12.5, and 25 μM), and incubated for another 24 h at 37°C. Cell viability was determined using the WST-8 assay as described above.

Influx and efflux of SU and Rho123 from SAL-treated HeLa cells

Cells (5×10^5) were cultured for 24 h in RPMI-1640 medium containing SAL (50 μg/mL), SAL (50 μg/mL)/saccharide (20 mM) or without SAL at 37°C in an atmosphere of 95% air/5% CO_2, supplemented with SU (3.12, 6.25 and 12.5 μM) or Rho123 (1 μM) and incubated for another 30 min. Influx of SU and Rho123 was detected using FACSCalibur (BD Biosciences) and an Olympus FV1000 confocal scanning microscope (Olympus). For studying SU and Rho123 efflux, cells (5×10^5) were cultured for 24 h in RPMI-1640 medium containing SAL (50 μg/mL), or without SAL at 37°C in an atmosphere of 95% air/5% CO_2, supplemented with SU (12.5 μM) or Rho123 (1 μM) and incubated for another 30 min. SU was removed from each well at 3 or 6 h intervals for a maximum of 24 h. Rho123 was removed from each well for 30 min. SU and Rho123 efflux was ascertained using FACSCalibur (BD Biosciences) and an Olympus FV1000 confocal scanning microscope (Olympus).

CRISPR/Cas9-mediated knockout of A4GALT

HeLa cells (1×10^6) were centrifuged and resuspended in 100 μL nucleofection V solution (Lonza, Basel, Switzerland) containing pRGEN-Human-A4GALT-U6 sgRNA vector (200 ng) and p3s-Cas9-Ef1a expression vector (200 ng) (ToolGen, Seoul, Korea) and electroporated with a Nucleofector (Lonza) using the I-13 program. After nucleofection, the cells were transferred to a 12-well plate containing 1 mL fresh complete medium (RPMI 1640 containing 10% FBS and antibiotic–antimycotic solution) and incubated at 37°C for 150 h. After incubation, the expression of Gb3 was detected using FACSCalibur (BD Biosciences) and TLC as described above.

Time series measurements of intracellular SU contents

Cells (1×10^4) were seeded in a CellCarrier™-96 microplates (PerkinElmer, Hamburg, Germany) and cultured in RPMI-1640 medium containing SAL (50 μg/mL) or without SAL at 37°C in an atmosphere of 95% air/5% CO_2. Before imaging, the cells were stained with Hoechst33342 (Dojindo Laboratories). The plate was scanned on Perkin Elmer Operetta CLS high-content imager using a 40× objective lens on confocal mode in a prewarmed live cell chamber set at 37°C in an atmosphere of 95% air/5% CO_2. Fluorescent images were captured in the Hoechst33342 channel at 488 nm before and at 3 min intervals after the addition of SU (final concentration 12.5 μM) for a maximum of 30 min. Subsequently, SU was removed from each well at 0.5 or 3 h intervals for a maximum of 24 h. Images were quantified using the Harmony software (PerkinElmer).

Analysis of intracellular accumulation site of SU

HeLa cells (1×10^4) were seeded in a 48-well flat-bottom plate (BD Falcon, Corning Life Sciences, MA) and incubated with SAL (50 μg/mL) for 0.5, 3, 9 or 18 h. Vacuole formation was observed using an EVOS FL Auto 2 cell imaging System (Thermo Fisher) in bright-field mode. For detecting lipid droplets, cells (1×10^4) were seeded in 24-well glass bottom culture plate (Iwaki EZView™, Asahi Techno Glass, Tokyo, Japan), incubated at 37°C in an atmosphere of 5% CO_2 for 24 h and then treated with SAL (50 μg/mL) for 24 h. Then, cells were fixed with 1% paraformaldehyde in D-PBS at 4°C for 15 min and washed thrice with D-PBS. The paraformaldehyde-fixed cells were treated with 0.1% Triton X-100 in D-PBS at 4°C for

15 min to permeabilize the cells. The permeabilized cells were treated with 0.5 μg/mL Nile Red (Wako, Osaka, Japan) at room temperature for 5 min. After washing, the cells were observed using a confocal scanning microscope (model FV1000; Olympus) with a 60× objective lens. For Neutral Red staining and LysoTracker Green DND-26 assay, HeLa cells (1×10^4) were seeded in 48-well flat-bottom culture plate (BD Falcon), incubated at 37°C in the presence of 5% CO_2 for 24 h and then treated with SAL (50 μg/mL) for 24 h and washed twice in D-PBS. These cells were then stained with Neutral Red (100 μg/mL, Wako, Osaka, Japan) and LysotTacker Green DND-26 (500 nM, Thermo Fisher) for 30 min under growth conditions. After washing, the cells were observed under a fluorescence microscope (EVOS FL Auto 2 Cell imaging system; Thermo Fisher). For the establishment of HeLa RFP-LAMP1 and HeLa GFP-LAMP1 cell lines, HeLa cells were treated with CellLight® Lysosome labeling BacMam 2.0-RFP and CellLight® Lysosome labeling BacMam 2.0-GFP (Thermo Fisher), respectively, according to the manufacturer's protocol. Twenty-four hours after treatment, the cells were cultured for 24 h in RPMI-1640 medium containing SAL (50 μg/mL) or without SAL at 37°C in an atmosphere of 95% air/5% CO_2, supplemented with SU (12.5 μM) and incubated for another 30 min. SU and LAMP1 exhibiting green and red fluorescence were acquired using a confocal scanning microscope (model FV1000; Olympus) with a 60× objective lens. Nuclei were counterstained with DRAQ5 (Biostatus Ltd, Leicestershire, UK). BFA (1 μg, Abcam, Cambridge, UK) was dissolved in 247 μL dimethyl sulfoxide to make a 10 mM stock solution. Cells were incubated with BFA (10 μM) in RPMI-1640 with FBS for 2 h, supplemented with SAL (50 μg/mL) and incubated for another 24 h. Bright-field images were acquired using a confocal scanning microscope (model FV1000; Olympus) with a 60× objective lens. For detecting LC3, cells (1×10^4) were seeded in 24-well glass bottom culture plate (Iwaki), incubated at 37°C in an atmosphere of 5% CO_2 for 24 h and then treated with SAL (50 μg/mL) for 24 h. Then, cells were fixed with 4% paraformaldehyde in D-PBS at room temperature for 15 min and washed thrice with D-PBS. The paraformaldehyde-fixed cells were treated with 0.1% Triton X-100 in D-PBS at room temperature for 15 min to permeabilize the cells. The cells were treated with anti-LC3 pAb (rabbit IgG; MBL) at a dilution of 1:500 in D-PBS (200 μL) at room temperature for 2 h and washed thrice with D-PBS. The cells were then treated with AF 546-conjugated goat anti-rabbit IgG (H + L) (Molecular Probes) at a dilution of 1:2000 in D-PBS (200 μL) at room temperature for 1 h. After washing, the cells were observed using a confocal scanning microscope (model FV1000; Olympus) with a 60× objective lens.

mRNA expression analysis

HeLa cells (5×10^5) were cultured for 24 h in RPMI-1640 medium containing SAL (50 μg/mL) or without SAL at 37°C in an atmosphere of 95% air/5% CO_2. Total RNA was extracted from cells using a Direct-zol RNA mini prep kit (Zymo Research Co., CA). cDNA was synthesized from the total RNA (1 μg) using a SuperScript VILO cDNA synthesis kit (Invitrogen, San Diego, CA). Quantitative reverse transcription-polymerase chain reaction (qRT-PCR) assays were performed using a LightCycler 480 system with the LightCycler 480 probes master kit (Roche Diagnostics, Indianapolis, IN). PCR primers for amplification of *SNX10* (forward: 5′-CGAAGAAGATATAGAGAATTCGTGTG-3′, reverse: 5′-GATGGAAGTTCTGGCAGTTGTA-3′) and *SNX11* (forward: 5′-GGAGCTGGTGCTGTTCTCA-3′, reverse: 5′-TCAGCCAATATGTACTGCCAAC-3′) were designed by the Universal Probe Library Assay Design Center (https://www.roche-applied-science.com/sis/rtpcr/upl/acenter.jsp) using a TaqMan/probe library assay. The expression levels of these genes were standardized relatively to the mRNA expression level of *GAPDH* (as a housekeeping gene) based on their average crossing point values.

Western blot analysis

HeLa cells (5×10^4) were cultured for 48 h in RPMI-1640 with (50 μg/mL) or without SAL at 37°C in an atmosphere of 95% air/5% CO_2 and lysed with ice-cold lysis buffer (10 mM Tris buffer [pH 7.5], 150 mM NaCl, 1% w/v TritonX-100, 5 mM ethylenediaminetetraacetic acid and complete protease inhibitor cocktail [Roche, Mannheim, Germany]) for 30 min at 4°C. The cell lysate was separated using sodium dodecyl sulfate-polyacrylamide gel electrophoresis (SDS-PAGE) (12.5% separation gel) and electrotransferred onto a polyvinylidene difluoride (PVDF) membrane (pore size 0.45 μm) (Hybond-P; GE Healthcare BioSciences AB, Uppsala, Sweden). The membrane was treated with blocking buffer (Blocking One; Nacalai Tesque Inc., Kyoto, Japan) for 1 h at room temperature and washed with Tris-buffered saline (TBS) containing 0.05% Tween-20. The primary antibodies used were against phospho-$MEK_{1/2}$ (1:1000, rabbit mAb; Cell Signaling Technology Inc., Danvers, MA [CST]), $MEK_{1/2}$ (1:1000, rabbit mAb; CST), phospho-$ERK_{1/2}$ (1:1000, rabbit mAb; CST), ERK1 (1:5000, mouse mAb; BD Biosciences) and GAPDH (1:20,000, mouse mAb; clone 6C5; Ambion/Invitrogen, Carlsbad, CA). These antibodies were applied in immunoreaction enhancer solution (Can Get Signal Solution 1; Toyobo Co., Osaka, Japan), and the membrane was incubated for 16 h at 4°C. The secondary antibody, horseradish peroxidase (HRP)-conjugated anti-mouse or anti-rabbit IgG (Chemicon International Inc., Temecula, CA), was diluted 1:20,000 in immunoreaction enhancer solution, applied on the membrane and incubated for 1 h at room temperature. The membrane was exposed to X-ray film (Fuji Film Co., Tokyo, Japan) after treatment with enhanced chemiluminescence (ECL) Prime detection reagent (GE Healthcare BioSciences AB).

Internalization of SAL into HeLa

SAL was labeled using HiLyte Fluor™ 555 (HL) labeling kit-NH_2 (Dojindo) according to the instruction manual. HeLa cells (1×10^4) were seeded in 24-well glass bottom culture plate (Iwaki), incubated at 37°C in an atmosphere of 5% CO_2 for 24 h and then treated with HL-SAL (50 μg/mL) for 24 h. After washing, the cells were observed using a confocal scanning microscope (model FV1000; Olympus) with a 60× objective lens.

Statistical analysis

Experimental results are presented as mean ± standard error (SE). Differences in means were evaluated using the two-tailed Student's *t*-test, with P values <0.05 considered statistically significant.

Supplementary data

Supplementary data for this article is available online at http://glycob.oxfordjournals.org/.

Acknowledgments

We thank Editage (www.editage.jp) for English language editing.

Funding

This work was supported by the Ministry of Education, Culture, Sports, Science and Technology (MEXT) of Japan.

Conflict of interest

The authors declare that there are no conflicts of interest regarding the publication of this paper.

Author contributions

S. Sugawara, M. Takayanagi and S. Honda conducted all experiments and analyzed the data. S. Sugawara and M. Takayanagi wrote the manuscript. M. Hosono contributed to manuscript revision. Y. Fujii and Y. Ozeki provided a sample. T. Tatsuta., Y. Ozeki., J. Ito, M. Sato and M. Hosono supervised all experiments. All authors read and approved the final manuscript.

Abbreviations

A4GALT, α1,4-galactosyltransferase; ABC, ATP-binding cassette; ABCG2, ABC subfamily G member 2; AF, Alexa Fluor; ATP, adenosine triphosphate; BCRP, breast cancer resistance protein; BFA, brefeldin A; c-kit, tyrosine protein kinase kit; ConA, concanavalin A; CPT-11, irinotecan; D-PBS, Dulbecco's phosphate-buffered saline; Dox, doxorubicin; ECL, enhanced chemiluminescence; ERK, extracellular signal-regulated kinase; FBS, fetal bovine serum; FITC, fluorescein isothiocyanate; Gb3, globotriaosylceramide; GEM, glycosphingolipid-enriched microdomains; GFP, green fluorescence protein; HPTLC, high-performance TLC; HRP, horseradish peroxidase; LAMP1, lysosomal-associated membrane protein 1; mAb, monoclonal antibody; MEK, mitogen-activated protein/extracellular signal-regulated kinase; mRCC, metastatic renal cell carcinoma; MRP1, multidrug resistance-associated protein 1; MytiLec, mussel *Mytilus galloprovincialis* lectin; PDGFR, platelet-derived growth factor receptor; P-gp, P-glycoprotein; PI, propidium iodide; PVDF, polyvinylidene difluoride; PX, phox homology; pAb, polyclonal antibody; qRT-PCR, quantitative reverse transcription-polymerase chain reaction; RBL, rhamnose-binding lectin; RFP, red fluorescence protein; rhodamine123, Rho123; RPMI, Roswell Park Memorial Institute; SAL, *Silurus asotus* egg lectin; SDS-PAGE, sodium dodecyl sulfate-polyacrylamide gel electrophoresis; SE, standard error; SNX, sorting nexin; SU, sunitinib; TBS, Tris-buffered saline; TK, tyrosine kinase; VEGFR, vascular endothelial growth factor receptor; VBL, vinblastine; WGA, wheat germ agglutinin; LDH, lactate dehydrogenase

References

Abrams TJ, Lee LB, Murray LJ, Pryer NK, Cherrington JM. 2003. SU11248 inhibits KIT and platelet-derived growth factor receptor beta in preclinical models of human small cell lung cancer. *Mol Cancer Ther*. 2:471–478.

Aparicio-Gallego G, Blanco M, Figueroa A, García-Campelo R, Valladares-Ayerbes M, Grande-Pulido E, Antón-Aparicio L. 2011. New insights into molecular mechanisms of sunitinib-associated side effects. *Mol Cancer Ther*. 10:2215–2223.

Boegemann M, Hubbe M, Thomaidou D, Blackburn S, Bent-Ennakhil N, Wood R, Bargo D. 2018. Sunitinib treatment modification in first-line metastatic renal cell carcinoma: Analysis of the STAR-TOR registry. *Anticancer Res*. 38:6413–6422.

Carelle N, Piotto E, Bellanger A, Germanaud J, Thuillier A, Khayat D. 2002. Changing patient perceptions of the side effects of cancer chemotherapy. *Cancer*. 95:155–163.

Croci DO, Cerliani JP, Pinto NA, Morosi LG, Rabinovich GA. 2014. Regulatory role of glycans in the control of hypoxia-driven angiogenesis and sensitivity to anti-angiogenic treatment. *Glycobiology*. 24:1283–1290.

Cullen PJ. 2008. Endosomal sorting and 29chinate29: An emerging role for sorting nexins. *Nat Rev Mol Cell Biol*. 9:574–582.

Demetri GD, van Oosterom AT, Garrett CR, Blackstein ME, Shah MH, Verweij J, McArthur G, Judson IR, Heinrich MC, Morgan JA, et al. 2006. Efficacy and safety of sunitinib in patients with advanced gastrointestinal stromal tumour after failure of imatinib: A randomized controlled trial. *Lancet*. 368:1329–1338.

Di Desidero T, Antonelli A, Orlandi P, Ferrari SM, Fioravanti A, Alì G, Fontanini G, Basolo F, Francia G, Bocci G. 2017. Synergistic efficacy of irinotecan and sunitinib combination in preclinical models of anaplastic thyroid cancer. *Cancer Lett*. 411:35–43.

Domenichini A, Adamska A, Falasca M. 2019. ABC transporters as cancer drivers: Potential functions in cancer development. *Biochim Biophys Acta Gen Subj*. 1863:52–60.

Fujii Y, Sugawara S, Araki D, Kawano T, Tatsuta T, Takahashi K, Kawsar SM, Matsumoto R, Kanaly RA, Yasumitsu H, et al. 2012a. MRP1 expressed on Burkitt's lymphoma cells was depleted by catfish egg lectin through Gb3-glycosphingolipid and enhanced cytotoxic effect of drugs. *Protein J*. 31:15–26.

Fujii Y, Dohmae N, Takio K, Kawsar SM, Matsumoto R, Hasan I, Koide Y, Kanaly RA, Yasumitsu H, Ogawa Y, et al. 2012b. A lectin from the mussel *Mytilus galloprovincialis* has a highly novel primary structure and induces glycan-mediated cytotoxicity of globotriaosylceramide-expressing lymphoma cells. *J Biol Chem*. 287:44772–44783 287(53.

Fujiwara T, Oda K, Yokota S, Takatsuki A, Ikehara Y. 1988. Brefeldin A causes disassembly of the Golgi complex and accumulation of secretory proteins in the endoplasmic reticulum. *J Biol Chem*. 263:18545–18552.

Gotink KJ, Broxterman HJ, Labots M, de Haas RR, Dekker H, Honeywell RJ, Rudek MA, Beerepoot LV, Musters RJ, Jansen G, et al. 2011. Lysosomal sequestration of sunitinib: A novel mechanism of drug resistance. *Clin Cancer Res*. 17:7337–7346.

Hatakeyama T, Nagatomo H, Yamasaki N. 1995. Interaction of the hemolytic lectin CEL-III from the marine invertebrate Cucumaria 31chinate with the erythrocyte membrane. *J Biol Chem*. 270:3560–3564.

Hatakeyama T, Furukawa M, Nagatomo H, Yamasaki N, Mori T. 1996. Oligomerization of the hemolytic lectin CEL-III from the marine invertebrate *Cucumaria 31chinate* induced by the binding of carbohydrate ligands. *J Biol Chem*. 271:16915–16920.

Hosono M, Kawauchi H, Nitta K, Takayanagi Y, Shiokawa H, Mineki R, Murayama K. 1993. Purification and characterization of *Silurus asotus* (catfish) roe lectin. *Biol Pharm Bull*. 16:1–5.

Hosono M, Ishikawa K, Mineki R, Murayama K, Numata C, Ogawa Y, Takayanagi Y, Nitta K. 1999. Tandem repeat structure of rhamnose-binding lectin from catfish (*Silurus asotus*) eggs. *Biochim Biophys Acta Gen Subj*. 1472:668–675.

Hosono M, Sugawara S, Tatsuta T, Hikita T, Kominami J, Nakamura-Tsuruta S, Hirabayashi J, Kawsar SM, Ozeki Y, Hakomori SI, et al. 2013. Domain composition of rhamnose-binding lectin from shishamo smelt eggs and its carbohydrate-binding profiles. *Fish Physiol Biochem*. 39: 1619–1630.

Ivanova L, Uhlig S. 2008. A bioassay for the simultaneous measurement of metabolic activity, membrane integrity, and lysosomal activity in cell cultures. *Anal Biochem*. 379:16–19.

Kawano T, Sugawara S, Hosono M, Tatsuta T, Ogawa Y, Fujimura T, Taka H, Murayama K, Nitta K. 2009. Globotriaosylceramide-expressing Burkitt's lymphoma cells are committed to early apoptotic status by rhamnose-binding lectin from catfish eggs. *Biol Pharm Bull*. 32:345–353.

Kovbasnjuk O, Mourtazina R, Baibakov B, Wang T, Elowsky C, Choti MA, Kane A, Donowitz M. 2005. The glycosphingolipid globotriaosylceramide in the metastatic transformation of colon cancer. *Proc Natl Acad Sci USA*. 102:19087–19092.

Kunimatsu S, Mizuno T, Fukudo M, Katsura T. 2013. Effect of P-glycoprotein and breast cancer resistance protein inhibition on the pharmacokinetics of sunitinib in rats. *Drug Metab Dispos*. 41:1592–1597.

Lanne B, Jondal M, Karlsson KA. 1996. Galα4Gal-binding antibodies: Specificity and use for the mapping of glycolipids of Burkitt lymphoma and other human tumors. *Glycobiology*. 6:423–431.

Lin J, Shi SS, Zhang JQ, Zhang YJ, Zhang L, Liu Y, Jin PP, Wei PF, Shi RH, Zhou W, et al. 2016. Giant cellular vacuoles induced by rare earth oxide nanoparticles are abnormally enlarged endo/lysosomes and promote mTOR-dependent TFEB nucleus translocation. *Small*. 12: 5759–5768.

Maak M, Nitsche U, Keller L, Wolf P, Sarr M, Thiebaud M, Rosenberg R, Langer R, Kleeff J, Friess H, et al. 2011. Tumor-specific targeting of pancreatic cancer with Shiga toxin B-subunit. *Mol Cancer Ther*. 10:1918–1928.

Mendel DB, Laird AD, Xin X, Louie SG, Christensen JG, Li G, Schreck RE, Abrams TJ, Ngai TJ, Lee LB, et al. 2003. In vivo antitumor activity of SU11248, a novel tyrosine kinase inhibitor targeting vascular endothelial growth factor and platelet-derived growth factor receptors: Determination of a pharmacokinetic/pharmacodynamic relationship. *Clin Cancer Res*. 9:327–337.

Murayama K, Taka H, Kaga N, Fujimura T, Mineki R, Shindo N, Morita M, Hosono M, Nitta K. 1997. The structure of *Silurus asotus* (catfish) roe lectin (SAL): Identification of a noncovalent trimer by mass spectrometry and analytical ultracentrifugation. *Anal Biochem*. 247:319–326.

Nemoto R, Yamamoto S, Ogawa T, Naude R, Muramoto K. 2015. Effect of chum salmon egg lectin on tight junctions in Caco-2 cell monolayers. *Molecules*. 20:8094–8106.

Nowak-Sliwinska P, Weiss A, van Beijnum JR, Wong TJ, Kilarski WW, Szewczyk G, Verheul HM, Sarna T, van den Bergh H, Griffioen AW. 2015. Photoactivation of lysosomally sequestered sunitinib after angiostatic treatment causes vascular occlusion and enhances tumor growth inhibition. *Cell Death Dis*. 6:e1641.

Ohyama C, Fukushi Y, Satoh M, Saitoh S, Orikasa S, Nudelman E, Straud M, Hakomori S. 1990. Changes in glycolipid expression in human testicular tumor. *Int J Cancer*. 45:1040–1044.

Pratt J, Roy R, Annabi B. 2012. Concanavalin-A-induced autophagy biomarkers requires membrane type-1 matrix metalloproteinase intracellular signaling in glioblastoma cells. *Glycobiology*. 22:1245–1255.

Qin B, He M, Chen X, Pei D. 2006. Sorting nexin 10 induces giant vacuoles in mammalian cells. *J Biol Chem*. 281:36891–36896.

Raymond E, Dahan L, Raoul JL, Bang YJ, Borbath I, Lombard-Bohas C, Valle J, Metrakos P, Smith D, Vinik A, et al. 2011. Sunitinib malate for the treatment of pancreatic neuroendocrine tumors. *N Engl J Med*. 364:501–513.

Reaves B, Banting G. 1992. Perturbation of the morphology of the trans-Golgi network following brefeldin A treatment: Redistribution of a TGN-specific integral membrane protein, TGN38. *J Cell Biol*. 116: 85–94.

Saftig P, Klumperman J. 2009. Lysosome biogenesis and lysosomal membrane proteins: Trafficking meets function. *Nat Rev Mol Cell Biol*. 10:623–635.

Sawyers C. 2004. Targeted cancer therapy. *Nature*. 432:294–297.

Shin IS, Ishii S, Shin JS, Sung KI, Park BS, Jang HY, Kim BW. 2009. Globotriaosylceramide (Gb3) content in HeLa cells is correlated to Shiga toxin-induced cytotoxicity and Gb3 synthase expression. *BMB Rep*. 42:310–314.

Stimmer L, Dehay S, Nemati F, Massonnet G, Richon S, Decaudin D, Klijanienko J, Johannes L. 2014. Human breast cancer and lymph node metastases express Gb3 and can be targeted by STxB-vectorized chemotherapeutic compounds. *BMC Cancer*. 14:916.

Sugawara S, Hosono M, Ogawa Y, Takayanagi M, Nitta K. 2005a. Catfish egg lectin causes rapid activation of multidrug resistance 1 P-glycoprotein as a lipid translocase. *Biol Pharm Bull*. 28:434–441.

Sugawara S, Sasaki S, Ogawa Y, Hosono M, Nitta K. 2005b. Catfish (Silurus asotus) lectin enhances the cytotoxic effects of doxorubicin. *Yakugaku Zasshi*. 125:327–334.

Sugawara S, Araya K, Hosono M, Tatsuta T, Nitta K. 2011. Combination effect of catfish lectin and anti-cancer drugs on Raji and K562 cells. *J Tohoku Pharm Univ*. 58:41–46.

Sugawara S, Im C, Kawano T, Tatsuta T, Koide Y, Yamamoto D, Ozeki Y, Nitta K, Hosono M. 2017. Catfish rhamnose-binding lectin induces $G_{0/1}$ cell cycle arrest in Burkitt's lymphoma cells via membrane surface Gb3. *Glycoconj J*. 34:127–138.

Tekisogullari K, Topcul M. 2013. The effects of sunitinib malate used in targeted therapy on the proliferation of HeLa cells in vitro. *J BUON*. 18:253–260.

Tsai TL, Wang HC, Hung CH, Lin PC, Lee YS, Chen HHW, Su WC. 2017. Wheat germ agglutinin-induced paraptosis-like cell death and protective autophagy is mediated by autophagy-linked FYVE inhibition. *Oncotarget*. 8:91209–91222.

Tsujimoto Y. 1997. Apoptosis and necrosis: Intracellular ATP level as a determinant for cell death modes. *Cell Death Differ*. 4:429–434.

Unno H, Goda S, Hatakeyama T. 2014. Hemolytic lectin CEL-III heptamerizes via a large structural transition from α-helices to a β-barrel during the transmembrane pore formation process. *J Biol Chem*. 289:12805–12812.

Xu J, Xu T, Wu B, Ye Y, You X, Shu X, Pei D, Liu J. 2013. Structure of sorting nexin 11 (SNX11) reveals a novel extended phox homology (PX) domain critical for inhibition of SNX10-induced vacuolation. *J Biol Chem*. 288:16598–16605.

Yamashita K, Kawai Y, Tanaka Y, Hirano N, Kaneko J, Tomita N, Ohta M, Kamio Y, Yao M, Tanaka I. 2011. Crystal structure of the octameric pore of staphylococcal γ-hemolysin reveals the β-barrel pore formation mechanism by two components. *Proc Natl Acad Sci U S A*. 108: 17314–17319.

Wei F, Cao S, Ren X, Liu H, Yu J, Li H, Hao X. 2008. Efficient antiproliferative and antiangiogenic effects on human ovarian cancer growth by gene transfer of attenuated mutants of Shiga-like toxin I. *Int J Gynecol Cancer*. 18:677–691.